# **PCCP**



### **PAPER**



Cite this: Phys. Chem. Chem. Phys., 2019, 21, 20764

Received 4th August 2019, Accepted 4th September 2019

DOI: 10.1039/c9cp04322e

rsc.li/pccp

# Direct detection of polar structure formation in helium nanodroplets by beam deflection measurements†

John W. Niman, pa Benjamin S. Kamerin, Lorenz Kranabetter, Daniel J. Merthe, Jiří Suchan, Petr Slavíček \*\* and Vitaly V. Kresin \*\* \*\* And Vitaly V. Kresin \*\* \*\* Daniel J. Merthe, \*\* Tanabetter, Daniel J. Merthe, \*\* Dani

Long-range intermolecular forces are able to steer polar molecules submerged in superfluid helium nanodroplets into highly polar metastable configurations. We demonstrate that the presence of such special structures can be identified, in a direct and determinative way, by electrostatic deflection of the doped nanodroplet beam. The measurement also establishes the structures' electric dipole moments. In consequence, the introduced approach is complementary to spectroscopic studies of low-temperature molecular assembly reactions. It is enabled by the fact that within the cold superfluid matrix the molecular dipoles become nearly completely oriented by the applied electric field. As a result, the massive (tens of thousands of helium atoms) nanodroplets undergo significant deflections. The method is illustrated here by an application to dimers and trimers of dimethyl sulfoxide (DMSO) molecules. We interpret the experimental results with *ab initio* theory, mapping the potential energy surface of DMSO complexes and simulating their low temperature aggregation dynamics.

### 1. Introduction

Long-range intermolecular forces play an essential role in reactions at sub-Kelvin temperatures (see, *e.g.*, the reviews in ref. 1–4). For example, long-range interactions between polar molecules embedded in helium nanodroplets often dominate the outcome of their assembly reactions. This is facilitated by the low internal temperature (370 mK) of the nanodroplet medium as well as by its superfluidity.<sup>5</sup> As a result, molecular reorientation and intermolecular reactions within nanodroplets are not perturbed by inhomogeneities present in other low-temperature surface and matrix isolation environments, making these "nano-cryo-traps" excellent hosts for exploring the physics and chemistry of cold molecular systems.<sup>6</sup>

A landmark demonstration of the action of long-range forces was furnished by experiments on HCN molecules sequentially picked up by a He nanodroplet beam.<sup>7</sup> These linear molecules

were guided by dipole–dipole forces to self-assemble into long chains aligned head-to-tail inside the nanodroplet. HCCCN was found to behave similarly. These chains rank among the most polar molecular systems ever observed in a molecular beam. In an "ordinary" environment thermal motion would drive them out of this type of metastable configuration, but within a very cold and inert liquid helium droplet they become long-lived. Data on formic acid, imidazole, and acetic acid dimers suggested an analogous alignment mechanism.

However, such an outcome is not universal in nanodroplet embedding. For example, two HCl molecules arrange themselves nearly at a right angle to each other<sup>13,14</sup> while water clusters form cyclic structures.<sup>15</sup> The "decision" by polar molecules how to orient themselves upon approach depends on the strength of their dipoles, on their responsiveness to the mutually reorienting torques (*i.e.*, their rotational constants and their accessible rotational quantum states), and on the directionality and flexibility of their bond formation. That is to say, the outcome depends on the shape of the intermolecular potential energy surface and on the barrier heights encountered on the path to the final configuration.

It is therefore interesting and informative to establish whether a molecular formation within a nanodroplet can reach its global energy minimum or finds itself trapped in a polar metastable state. However, often this is not a straightforward determination. The studies cited above based their conclusions on the interpretation of dopant infrared spectra or on inference

<sup>&</sup>lt;sup>a</sup> Department of Physics and Astronomy, University of Southern California, Los Angeles, CA 90089-0484, USA. E-mail: kresin@usc.edu

b Institut für Ionenphysik und Angewandte Physik, Universität Innsbruck, Technikerstr. 25, A-6020 Innsbruck, Austria

<sup>&</sup>lt;sup>c</sup> Department of Physical Chemistry, University of Chemistry and Technology, Technická 5, Prague 6, Czech Republic. E-mail: petr.slavicek@vscht.cz

<sup>&</sup>lt;sup>d</sup> J. Heyrovský Institute of Physical Chemistry v.v.i., The Czech Academy of Sciences, Dolejškova 3, 18223 Prague, Czech Republic

 $<sup>\</sup>dagger\,$  Electronic supplementary information (ESI) available. See DOI: 10.1039/c9cp04322e

<sup>‡</sup> Present address: Modern Electron, Bellevue, WA 98007, USA.

Paper PCCP

from electron attachment mass spectrometry. Such assignments grow more difficult and less definitive with increasing size and/or complexity of the embedded molecules and their assemblies.

In this work we describe a measurement which directly establishes the polarity of a molecular assembly, as well as determines its dipole moment. It makes use of electrostatic deflection of the doped nanodroplet beam. <sup>16,17</sup>

The technique is based on the fact that polar structures embedded within the superfluid matrix can be made nearly fully oriented by an external static electric field<sup>18</sup> and consequently experience an extremely large deflecting force from the field's gradient. Such a high degree of orientation is unattainable for bare polyatomic complexes in a molecular beam. Whereas some relatively small and light molecules reach rotational temperatures  $T_{\rm rot}$  below 1 K with the use of seeded supersonic expansions and exhibit large deflections (see, *e.g.*, ref. 19 and 20), this becomes impractical for heavier systems.

For the purpose of an estimate, consider the classical Langevin function for the orientation of a molecular rotor in an external field  $E\hat{z}$ :  $\bar{p}_z/p_0 = [\coth x - 1/x]$ . This is a good approximation<sup>21,22</sup> for  $k_BT_{\rm rot}\gg B$ . Here  $p_0$  is the molecule's dipole moment,  $\bar{p}_z$  is the average projection of this dipole on the field axis,  $x\equiv p_0E/k_BT_{\rm rot}$ , and B is the rotational constant. For  $T_{\rm rot}$  above a few K and practical electric field strengths, the ratio x remains small even for dipole moments of several Debye (D), and in this limit  $\bar{p}_z/p_0\approx x/3\ll 1$ . Therefore it is only when the rotational temperature becomes very low, as enabled in the present case by helium nanodroplet isolation, that the orientation can approach saturation ( $\bar{p}_z\to p_0$ ). This effect has been taken advantage of in landmark experiments using pendular-state spectroscopy. <sup>18</sup>

If the external electric field which orients the nanodroplet-submerged dipoles is designed also to have a collinear strong gradient, then these dipoles will experience such a strong side-ways force  $F_z = p_z(\partial E/\partial z)$  that the massive doped droplets, comprised of tens of thousands of helium atoms, will be significantly deflected in their entirety. Thus, our procedure involves comparing the deflection profile of a singly-doped nanodroplet beam with that of a beam composed of multiply-doped nanodroplets. If, for example, the droplets containing two (or three, *etc.*) molecules show negligible deflection, we can immediately conclude that the dimer (trimer, *etc.*) has settled into a nonpolar configuration. A strongly deflected profile, on the other hand, immediately attests to the formation of a polar structure, and the magnitude of the deflection translates into the magnitude of this formation's total dipole moment.

This is a conveniently unambiguous measurement applicable to a wide range of molecules, from diatomic to polyatomic (including biological). Practically any molecular species that can be brought into the vapor phase with a pressure of only  $10^{-6}$ – $10^{-4}$  mbar can be picked up by the nanodroplet beam and thermalized within the inert viscosity-free medium. The thermalization proceeds by evaporative cooling: the molecules' translational and internal energies are transferred to the superfluid matrix which has a very high thermal conductivity, and released *via* evaporation of surface helium atoms, promptly bringing the nanodroplet back to the original temperature.<sup>5</sup>

Here we apply the deflection method to monomers, dimers and trimers of the dimethyl sulfoxide molecule ("DMSO,"  $(CH_3)_2SO$ , molecular mass 78 Da). The molecule is nearly an oblate symmetric top, with rotational constants of<sup>23,24</sup> 0.235 cm<sup>-1</sup>, 0.231 cm<sup>-1</sup>, and 0.141 cm<sup>-1</sup> and its total dipole moment is<sup>25</sup> p=4.0 D. The measurement clearly reveals the presence of highly polar dimers and trimers, *i.e.*, the formation of metastable polar configurations abetted by the cryogenic nanodroplet environment. To our knowledge, this is the first direct non-spectroscopic identification of such a cold polar molecular assembly.

### 2. Results and discussion

### 2.1 Deflection profiles

The experimental setup has been described in detail elsewhere. <sup>16,17,26</sup> A nanodroplet beam is formed by cold nozzle expansion of pure helium gas. It passes first through a pick-up cell filled with DMSO vapor, and then between two high-voltage electrodes which create an electric field and a collinear field gradient directed perpendicular to the beam axis. Downstream, the beam enters through a slit into an electron-impact ionizer, and the intensities of the resulting molecular ions are recorded by a quadrupole mass spectrometer in synchronization with a beam chopper. The deflection induced by the electric field is determined by comparing the beam's "field-on" and "field-off" spatial profiles which are mapped out by translating the detector chamber, with its entrance slit, on a precision linear stage.

Molecules are picked up by helium nanodroplets via successive collisions in a Poisson process.<sup>5</sup> Therefore it is important to correlate measured beam deflections with the specific number of molecules embedded in the droplet. Dopants within nanodroplets are ionized indirectly via charge transfer to He<sup>+</sup> produced by electron bombardment; this transfer is a highly exothermic process which can cause fragmentation.<sup>27</sup> Consequently, when mapping out the deflection profile of a dopant ion peak in the mass spectrum, we need to ensure that it is not a fragment of a larger agglomerate. This is done by gradually increasing the vapor pressure in the pick-up cell and monitoring the mass spectrum for the appearance of molecular ions characteristic of progressively larger entities. For example, monomer ionization produces a strong (DMSO)<sup>+</sup> signal<sup>28</sup> at m = 78 Da, hence if we measure beam profiles with the mass spectrometer set to this mass peak but with the vapor pressure low enough to suppress the corresponding characteristic  $(DMSO)_2^+$  peak at m = 156 Da, then we can be confident that the deflection principally corresponds to droplets carrying the monomer. Similarly, profiles measured at m = 156 Da but before the appearance of the trimer's signal must derive from the dimer, etc. Representative mass spectra are shown in the ESI.†

Fig. 1 shows the deflection profiles of helium nanodroplets containing one, two, and three DMSO molecules. The deflections are substantial despite the fact that the droplets are truly massive ( $\sim 1 \times 10^4$ –3  $\times 10^4$  He atoms, as described in the caption). Therefore we are immediately and directly informed

PCCP Paper

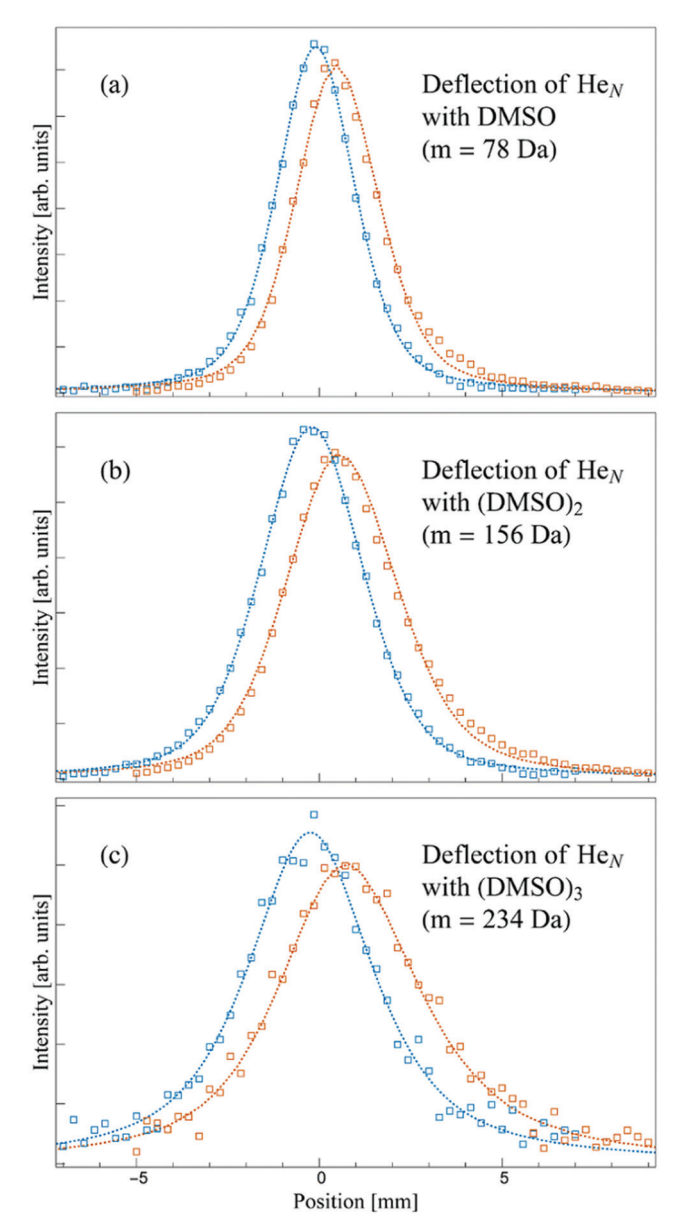


Fig. 1 Profiles of (DMSO)<sub>n</sub>-doped helium nanodroplet beams. Blue: zero-field profiles, orange: deflection by a field of 82 kV cm $^{-1}$  strength and 338 kV cm $^{-2}$  gradient. Symbols: experimental data, lines: fits of the deflection process, as described in the text. The monomer profile mapped for a particular temperature T and stagnation pressure P of the He $_N$  beam source is used to determine the average  $\bar{N}$  and width  $\Delta N$  of the nanodroplet size distribution, and then fits to the dimer and trimer profiles for the same source conditions yield these dopants' dipole moments. In (a) and (b) P=80 bar, T=15.5 K,  $\bar{N}\approx 2.3\times 10^4$ , in (c) P=80 bar, T=16.4 K,  $\bar{N}\approx 1.4\times 10^4$ . The gradual increase of the profile width with the number of dopant molecules is caused by transverse momentum transfer associated with each pick-up collision.

by Fig. 1(b) that (DMSO)<sub>2</sub> settles into a strongly polar configuration and not into its global minimum structure, because the latter would be symmetric with a zero dipole moment.<sup>29</sup>

In order to assign an absolute value of the dipole moment to the dopant, we must keep in mind that the host nanodroplets are not all of the same size. The size distribution produced by the nozzle expansion is log-normal, and this translates into a convolution of pick-up cross sections, deflection angles, and ionization efficiencies. Our procedure<sup>16,17</sup> is to start with the profile corresponding to a single DMSO dopant molecule whose dipole moment is known. A fit to the deflected profile (by a Monte Carlo simulation of the pick-up, evaporation, deflection, and detection steps) is used to calibrate the droplet size distribution. Then by repeating the deflection measurement and its simulation with doubly- and triply-doped nanodroplets produced and detected under the same conditions, we can deduce the electric dipole moments corresponding to the dimer and the trimer.

These dipole moments enter the fitting procedure at the step where the deflecting electrostatic force is calculated. As described in the Introduction, this requires knowing  $\bar{p}_z$ , i.e., the degree of orientation induced by the applied field. For the DMSO monomer this is carried out by diagonalizing the rotational Stark effect matrix (cf. ref. 30) using the components of the molecule's dipole moment.<sup>24</sup> For the heavier dimer and trimer the classical Langevin-Debye formula is sufficiently accurate.31 In calculating the monomer's Stark spectra one should keep in mind that rotational coupling to the superfluid<sup>32</sup> enhances the moments of inertia of the heavier molecular rotors by an average factor of  $\sim 2.5-3$  compared with their gas phase value.<sup>5,18</sup> Since DMSO's specific renormalization factor is not known, it was set to 2.6 in our data fitting procedure. We found that the inclusion of this factor had practically no effect on the deduced dipole of the dimer but shifted that of the trimer upward by  $\approx 10$ –15%. For the final fitted dipole values listed below, the (DMSO)<sub>n</sub> orientations within an applied 82 kV cm<sup>-1</sup> field were found to be 86%, 97%, and 98% for n = 1-3, respectively.

### 2.2 Dipole moments

From analysis of the measurements, we assign effective electric dipole moments of 7.2 D to  $(DMSO)_2$  and 8.6 D to  $(DMSO)_3$ , with an estimated accuracy of  $\pm 0.2$  D and  $\pm 0.6$  D, respectively. These values, which can be compared with the ground state moments of 0 D for the aforementioned symmetric dimer and 4.2 D for the trimer<sup>29</sup> (essentially a nonpolar dimer plus an unpaired monomer), establish the presence of highly polar metastable structures. In the cold superfluid environment these structures are steered into formation by the long-range intermolecular forces and are then unable to overcome the potential barrier leading to the global minimum configuration.

### 2.3 Modeling of molecular complex formation

To facilitate the interpretation of the above results, we supplemented the experiments with *ab initio* modeling of DMSO condensation. We optimized the geometry of DMSO dimers and trimers with the B3LYP functional with the aug-cc-pVDZ basis set. The DMSO complexes are dominantly bound by electrostatic forces but the dispersion interactions still play a non-negligible role. We have therefore used the D2 correction of Grimme.<sup>33</sup> The approach was tested against the CCSD(T)/aug-cc-pVTZ method for the DMSO dimer, yielding similar energetics (see the ESI†). All calculations were performed in the gas phase: by considering complexes with helium atoms

or within a dielectric continuum we found that the helium environment had a negligible effect on the structure and energetics. The potential energy surfaces (PES) were prescreened with molecular mechanics (MM)-based metadynamics simulations<sup>34</sup> and the structures were then recalculated at the DFT level (see the ESI† for further information).

The process of DMSO dimer formation was modeled with molecular dynamics (MD) simulations within the canonical ensemble. We used the Nosé-Hoover thermostat with a rather small value of  $\tau = 0.01$  ps. This corresponds to fast draining of extra energy from the system, so that at each time it essentially remains in equilibrium. A temperature of 5 K was chosen in order to accelerate the simulations. It is higher than in the experiment but the difference is small compared with the PES accuracy.

We started with two DMSO molecules positioned at a distance of 20 Å between the two sulphur atoms with a random orientation. We then performed molecular mechanics simulations with the MM force field.<sup>35</sup> The molecules gradually approached each other while aligning their dipole moment. Since the MM force field does not reproduce the energetics of the minima sufficiently well, at the intermolecular distance of 10 Å we reset the simulations, switching from the force field to the more accurate semiempirical density functional tight binding (DFTB) method<sup>36</sup> with D3 dispersion correction.<sup>37,38</sup> The system then continued to evolve in time for another 500 ps with a time step of 1 fs, using the velocity Verlet integrator. Dipoles along the path were recalculated at the B3LYP/aug-cc-pVDZ level.

The DFT and CCSD(T) calculations were performed in Gaussian09.<sup>39</sup> Molecular dynamics simulations were performed in GROMACS 2018.440 and the DFTB simulations in the DFTB+ 18.2 code.<sup>36</sup> We also utilized our in-house MD code ABIN.<sup>41</sup>

### 2.4 Results of modeling

Fig. 2 shows several low-lying minima of the DMSO dimer obtained from extensive mapping of its potential energy surface. The structures are divided into two classes of minima: nonpolar and polar. The global minimum (complex D1) of (DMSO)<sub>2</sub> has a symmetrical configuration with a zero dipole moment, consistent with the aforementioned work.<sup>29</sup> Structures D2 and D3 also belong to the low dipole manifold. Complexes D4 and D5 represent polar type structures. The experimental data suggest that the highly polar structure D5, with an almost orthogonal arrangement of dipoles, predominantly forms

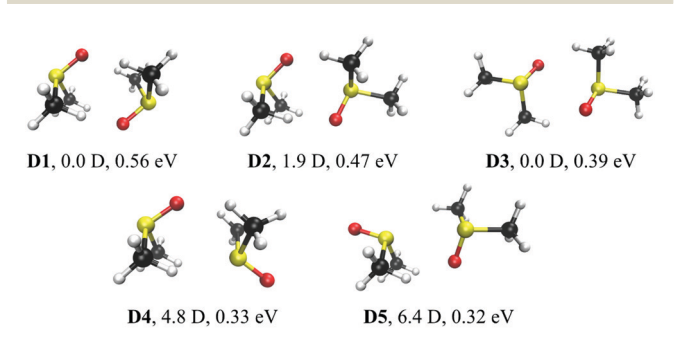


Fig. 2 Energy minima of the DMSO dimer, with their corresponding binding energies and dipole moments.

within nanodroplets. It is separated from the global minimum by a barrier of 0.08 eV (see the ESI†), which is more than sufficient to prevent a D5  $\rightarrow$  D1 transition.

Structure formation under cryogenic conditions is therefore likely to proceed as follows. At large separation the dominant force is the dipole-dipole interaction which aligns the two DMSO molecules. As described in the ESI,† there is a barrierless pathway between this structure and the D5 minimum. Therefore the molecules approach each other gradually within the helium environment to which all excess energy is almost immediately drained. The (DMSO)2 ends up trapped within the basin of complex D5.

We support this scenario by molecular dynamics (MD) simulations of the binary encounter under conditions of very efficient energy transfer to the environment, as specified above. At the start the two dipoles are assigned a random relative orientation, but the trajectory shown in Fig. 3 demonstrates that their orientation becomes correlated already at large

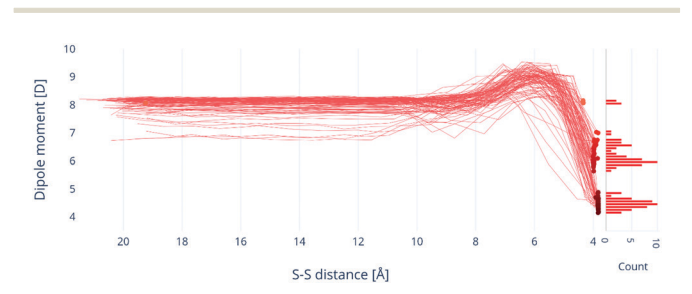


Fig. 3 Dipole moment of DMSO dimer complex along the intermolecular approach coordinate, as illustrated by a molecular dynamics simulation.

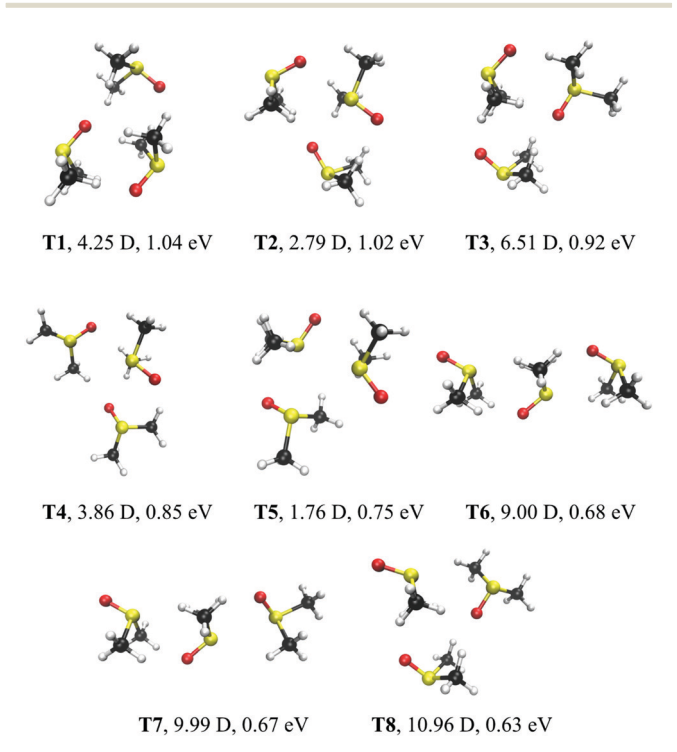


Fig. 4 Energy minima of DMSO trimers, with their corresponding binding energies and dipole moments.

PCCP Paper

distances. At closer approach the total dipole moment transiently increases. The molecular dipoles at that point are still parallel, hence the bump in the dipole moment is caused by mutual induction. Finally, the dimer quenches into one of the potential minima. In accord with the experiment, no formation of a zero dipole structure is found. The majority of the trajectories end up in the D5 minimum with a dipole of 6.4 D, some of them end up in the D4 minimum with a somewhat lower dipole moment than detected in the experiment.

The structures are more diverse for the trimer (Fig. 4). The lowest energy structure is cyclic with a dipole moment of 4.25 D (complex T1). Its formation is kinetically hindered. Indeed, as mentioned above, it represents the global dimer minimum to which the third molecule is added; since in the nanodroplets the former structure is not formed, neither will the cyclic trimer. We have located linear structures (T6, T7) with a much higher dipole close to 10 D. There are multiple other minima with intermediate dipoles. It follows from our simulations that a rather complex mixture of these metastable structures may be formed under the experimental conditions, and its precise assignment is beyond the reach of theory. The effective dipole moment of  $\approx 8.6$  D deduced from the deflection experiment represents the population average of the kinetically accessible structures.

### 3. Conclusion

In summary, we have demonstrated that the presence of peculiar polar structures, formed by sequential embedding of polar molecules into superfluid helium nanodroplets, can be clearly and directly detected by electrostatic deflection of the doped nanodroplet beam. In an application of this method to DMSO molecules we found that they form dipole-aligned dimer and trimer structures, steered by long-range electrostatic interactions. The formation mechanism and the magnitudes of the dipole moments are in good agreement with calculations describing molecular interactions and structure formation in the viscosity-free cryogenic environment.

In future applications it will be interesting to extend this approach, for example, to a study of interactions between polar amino acids or between prototype solute and solvent molecules, as well as between molecules in photoinduced polar conformations. It is also interesting to inquire whether transfer of angular momentum between the impurities and the quantum-fluid bath, a phenomenon predicted to have the potential to screen the impurity – electric field interaction, <sup>42</sup> may be able to measurably affect the dynamics of molecular assembly within nanodroplets.

### Conflicts of interest

There are no conflicts to declare.

# Acknowledgements

This work was supported by the U. S. National Science Foundation under Grant No. CHE-1664601. L. K. acknowledges a

scholarship from the Austrian Marshall Plan Foundation and support from the Austrian Science Fund under project FWF W1259. J. S. and P. S. thank the Czech Science Foundation for support under Project number 18-16577S. J. S. is an International Max Planck Research School for Many Particle Systems in Structured Environments student. We would like to thank Jiahao Liang and Atef Sheekhoon for assistance.

### References

- 1 M. T. Bell and T. P. Softley, *Mol. Phys.*, 2009, **107**, 99–132
- 2 M. Schnell and G. Meijer, Angew. Chem., Int. Ed., 2009, 48, 6010–6031.
- 3 G. Quéméner and P. S. Julienne, Chem. Rev., 2012, 112, 4949–5011.
- 4 N. Balakrishnan, J. Chem. Phys., 2016, 145, 150901.
- 5 J. P. Toennies and A. F. Vilesov, Angew. Chem., Int. Ed., 2004, 43, 2622–2648.
- 6 K. K. Lehmann and G. Scoles, Science, 1998, 279, 2065–2066.
- 7 K. Nauta and R. E. Miller, Science, 1999, 283, 1895-1897.
- 8 K. Nauta, D. T. Moore and R. E. Miller, *Faraday Discuss.*, 1999, **113**, 261–278.
- 9 F. Madeja, M. Havenith, K. Nauta, R. E. Miller, J. Chocholoušová and P. J. Hobza, *Chem. Phys.*, 2004, 120, 10554–10560.
- 10 M. Y. Choi and R. E. Miller, J. Phys. Chem. A, 2006, 110, 9344–9351.
- 11 F. Ferreira da Silva, S. Jaksch, G. Martins, H. M. Dang, M. Dampc, S. Denifl, T. D. Märk, P. Limão-Vieira, J. Liu, S. Yang, A. M. Ellis and P. Scheier, *Phys. Chem. Chem. Phys.*, 2009, 11, 11631–11637.
- 12 J. A. Davies, M. W. D. Hanson-Heine, N. A. Besley, A. Shirley, J. Trowers, S. Yang and A. M. Ellis, *Phys. Chem. Chem. Phys.*, 2019, 21, 13950–13958.
- 13 M. Ortlieb, Ö. Birer, M. Letzner, G. W. Schwaab and M. Havenith, *J. Phys. Chem. A*, 2007, **111**, 12192–12199.
- 14 D. Skvortsov, R. Sliter, M. Y. Choi and A. F. Vilesov, *J. Chem. Phys.*, 2007, **128**, 094308.
- 15 K. Nauta and R. E. Miller, Science, 2000, 287, 293-295.
- 16 D. J. Merthe and V. V. Kresin, *J. Phys. Chem. Lett.*, 2016, 7, 4879–4883.
- 17 J. W. Niman, B. S. Kamerin, D. J. Merthe, L. Kranabetter and V. V. Kresin, *Phys. Rev. Lett.*, 2019, **123**, 043203.
- 18 M. Y. Choi, G. E. Douberly, T. M. Falconer, W. K. Lewis, C. M. Lindsay, J. M. Merritt, P. L. Stiles and R. E. Miller, *Int. Rev. Phys. Chem.*, 2006, 25, 15–75.
- 19 Y.-P. Chang, D. Horke, S. Trippel and J. Küpper, *Int. Rev. Phys. Chem.*, 2015, 34, 557–590.
- 20 M. Johny, J. Onvlee, T. Kierspel, H. Bieker, S. Trippel and J. Küpper, *Chem. Phys. Lett.*, 2019, 721, 149–152.
- 21 B. Friedrich and D. Herschbach, *Int. Rev. Phys. Chem.*, 1996, 15, 325–344.
- 22 J. Bulthuis, J. A. Becker, R. Moro and V. V. Kresin, *J. Chem. Phys.*, 2008, **129**, 024101.

Paper PCCP

23 W. Feder, H. Dreizler, H. D. Rudolph and V. Typke, Z. Naturforsch., A: Phys. Sci., 1969, 24, 266–278.

- 24 M. L. Senent, S. Dalbouha, A. Cuisset and D. Sadovskii, *J. Phys. Chem. A*, 2015, **119**, 9644–9652.
- 25 CRC Handbook of Chemistry and Physics, ed. J. R. Rumble, CRC Press, Boca Raton, 99th edn, 2018.
- 26 D. J. Merthe, PhD thesis, University of Southern California, 2017.
- 27 A. Mauracher, O. Echt, A. M. Ellis, S. Yang, D. K. Bohme, J. Postler, A. Kaiser, S. Denifl and P. Scheier, *Phys. Rep.*, 2018, 751, 1–90.
- 28 NIST Chemistry WebBook, NIST Standard Reference Database Number 69, ed. P. J. Linstrom and W. G. Mallard, National Institute of Standards and Technology, Gaithersburg, 2018, http://webbook.nist.gov (accessed May 2019).
- 29 N. S. Venkataramanan, A. Suvitha and Y. Kawazoe, *J. Mol. Liq.*, 2018, **249**, 454–462.
- 30 Y.-P. Chang, F. Filsinger, B. G. Sartakov and J. Küpper, Comput. Phys. Commun., 2014, 185, 339–349.
- 31 L. Pei, J. Zhang and W. Kong, *J. Chem. Phys.*, 2007, 127, 174308.

- 32 M. Lemeshko, Phys. Rev. Lett., 2017, 118, 095301.
- 33 S. Grimme, J. Comput. Chem., 2006, 27, 1787-1799.
- 34 A. Barducci, M. Bonomi and M. Parrinello, WIREs Comput. Mol. Sci., 2011, 1, 826–843.
- 35 M. L. Strader and S. E. Feller, J. Phys. Chem. A, 2002, 106, 1074–1080.
- 36 B. Aradi, B. Hourahine and Th. Frauenheim, *J. Phys. Chem. A*, 2007, **111**, 5678–5684.
- 37 S. Grimme, J. Antony, S. Ehrlich and H. Krieg, *J. Chem. Phys.*, 2010, **132**, 154104.
- 38 S. Grimme, S. Ehrlich and L. Goerigk, *J. Comput. Chem.*, 2011, 32, 1456–1465.
- 39 M. J. Frisch, et al., Gaussian 09 (Rev. D.01), Gaussian, Inc., Wallingford, CT, 2009.
- 40 M. J. Abraham, T. Murtola, R. Schulz, S. Páll, J. C. Smith, B. Hess and E. Lindahl, *SoftwareX*, 2015, 1–2, 19–25.
- 41 ABIN, Molecular Dynamics program. Source code available at https://github.com/photox/abin. , DOI: 10.5281/zenodo. 1228462.
- 42 E. Yakaboylu and M. Lemeshko, *Phys. Rev. Lett.*, 2017, **118**, 085302.

### SUPPORTING INFORMATION FOR

# Direct detection of polar structure formation in helium nanodroplets by beam deflection measurements

John W. Niman,<sup>a</sup> Benjamin S. Kamerin,<sup>a</sup> Lorenz Kranabetter,<sup>b</sup> Daniel J. Merthe,<sup>a</sup> Jiří Suchan,<sup>c</sup> Petr Slavíček,<sup>cd</sup> Vitaly V. Kresin<sup>a</sup>

### Contents

- I.  $(DMSO)_n$  ion mass spectra
- II. Ab initio calculations: Benchmarking
- III. Mapping of the (DMSO)<sub>2</sub> and (DMSO)<sub>3</sub> potential energy surfaces
- IV. Transition between two dimers at a distance and D5
- V. Transition between the D5 and D1 minima
- VI. Two dimensional free energy surface
- VII. Force field parameters
- VIII. Cartesian coordinates of all structures

### References

<sup>&</sup>lt;sup>a</sup> Department of Physics and Astronomy, University of Southern California, Los Angeles, CA 90089-0484, USA

<sup>&</sup>lt;sup>b</sup> Institut für Ionenphysik und Angewandte Physik, Universität Innsbruck, Technikerstr. 25, A-6020 Innsbruck, Austria

<sup>&</sup>lt;sup>c</sup> Department of Physical Chemistry, University of Chemistry and Technology, Technická 5, Prague 6, Czech Republic

<sup>&</sup>lt;sup>d</sup> J. Heyrovský Institute of Physical Chemistry v.v.i., The Czech Academy of Sciences, Dolejškova 3, 18223 Prague, Czech Republic

### I. (DMSO)<sub>n</sub> ion mass spectra

As described in the main text, deflection profiles of droplets doped with DMSO monomers, dimers, or trimers were acquired by setting the mass spectrometer to the masses of (DMSO)<sup>+</sup>, (DMSO)<sub>2</sub><sup>+</sup> and (DMSO)<sub>3</sub><sup>+</sup> ions, respectively, and maintaining the pickup vapor pressure at a level such that the mass peak of interest would be dominant over the next higher one. This is illustrated in Fig. S1. The mass spectrometer is a Balzers QMG-511 crossed-beam quadrupole analyzer with its electron impact ionization source set to 90 eV impact energy.

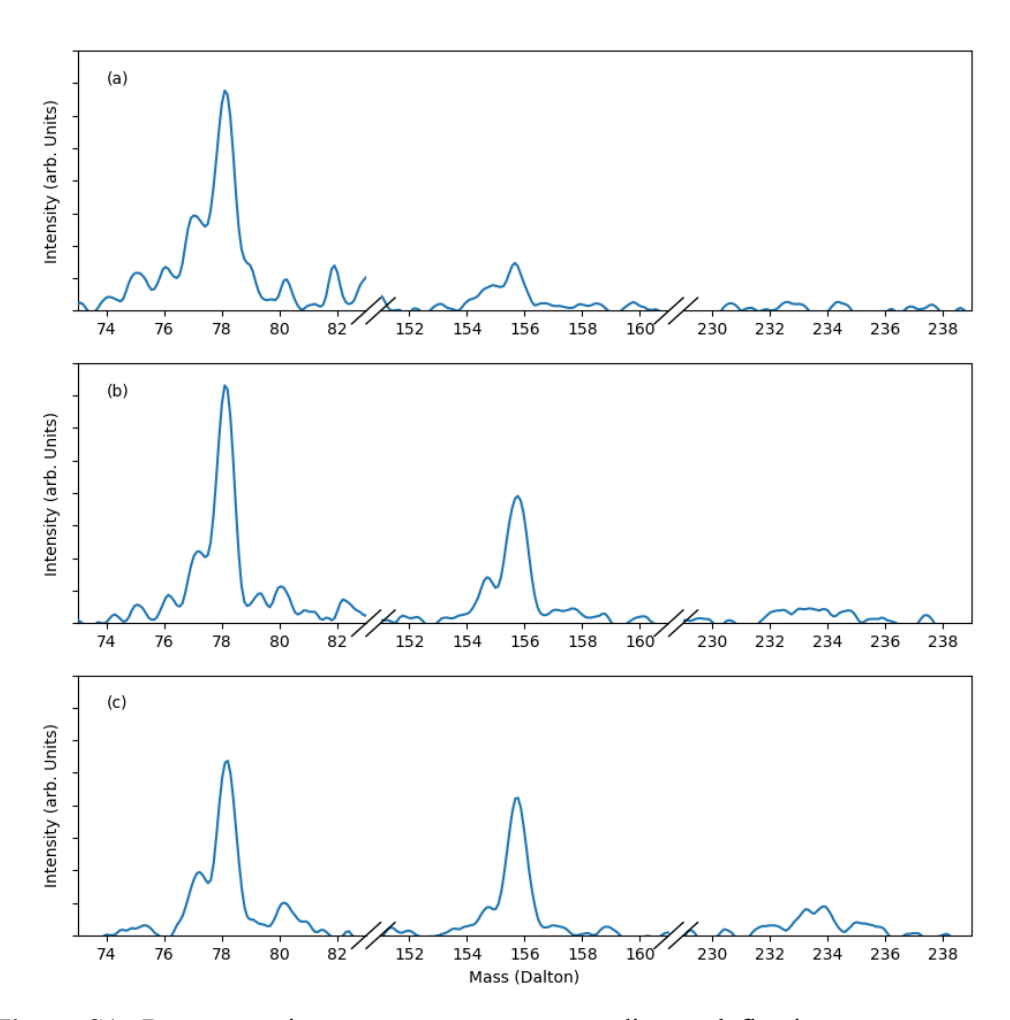


**Figure S1.** Representative mass spectra corresponding to deflection measurements on  $(DMSO)_n$ -doped nanodroplets. The mass spectrometer was set to the masses of intact ions: (a) 78 Da for the monomer, (b) 156 Da for the dimer, (c) 234 Da for the trimer.

### II. Ab initio calculations: Benchmarking

The potential energy surface was explored with the B3LYP(D2)/aug-cc-pVDZ method. The dipole moment of the isolated DMSO molecule in its equilibrium geometry calculated with this approach was 4.3 D, which is consistent with the tabulated value soft 4.0 D within the expected accuracy of DFT. We validated this approach against the high-level CCSD(T)/aug-cc-pVTZ method. Basis set superposition error (BSSE) correction was used for all structures. The agreement is very good for all cluster structures, see Table S1. We also show the energetics of the respective minima at the DFTB/D3 level used for exploratory simulations. The DFT and CCSD(T) calculations were performed in the Gaussian 09, rev. D01 package, the DFTB results were calculated in the DFTB+ 18.2 program. S4

**Table S1.** Comparison of DMSO dimer binding energies at the CCSD(T), B3LYP(D2) and DFTB(D3) levels. The BSSE correction was accounted for in the CCSD(T) and B3LYP(D2) calculations.

Dimer	Binding energy [eV]		
complex	CCSD(T)/aug-cc-pVTZ	B3LYP/aug-cc-pVDZ D2	DFTB
<b>D</b> 1	0.53	0.56	0.46
<b>D2</b>	0.46	0.47	0.41
D3	0.40	0.39	0.36
<b>D</b> 4	0.33	0.33	0.28
D5	0.32	0.32	0.26

### III. Mapping of the (DMSO)<sub>2</sub> and (DMSO)<sub>3</sub> potential energy surfaces

The potential energy surfaces (PES) of DMSO complexes are rather rich and we mapped them in the following way. First, we performed accelerated molecular dynamics simulations with the molecular mechanics (MM) force field, so using the so-called metadynamics method. Here, an additional potential is added along a preselected coordinate so that we can quickly overcome barriers along these coordinates. These simulations then also provide the free energy as a function of the selected coordinate [potential of mean force (PMF) or free energy surface (FES)]. We then selected different structures with distinct dipole moments from these metadynamical trajectories and performed further B3LYP optimization.

Metadynamics simulations were performed at 100 K to reveal the regions of interest in the dipole moment coordinate. This temperature is much higher than the experimental conditions, yet we opted for it to avoid ergodicity problems. Note that these simulations are only auxiliary, serving as a starting point for minimizations or MD simulations. The minimum on the PMF is found for a small yet non-zero dipole moment due to entropic reasons. The force field overestimates the dipole moment by 20% with respect to the *ab initio* value. The final PMFs for the dimer and trimer complexes are displayed in Fig. S2.

By clustering structures with similar dipoles together and performing 100 subsequent optimizations with Gaussian 09, for both the dimer and trimer structures, we were then able to map their PES landscapes.

The metadynamics parameters were as follows. The dimer simulation length was 100 ps, leap-frog stochastic integrator was utilized, the temperature was set to 100 K with a thermostat constant of  $\tau$  =1.0 ps. For the trimer the simulation length was increased to 300 ps. The collective variable (CV) is the total dipole moment. An additional Gaussian potential was added every 100 steps. The Gaussian height was 0.015 kJ/mol and the CV gaussian width was 1.2 Debye.

MD simulations were performed with GROMACS 2018.4 code<sup>S7</sup> coupled with PLUMED 2.5 code<sup>S8</sup> for the FES simulations.

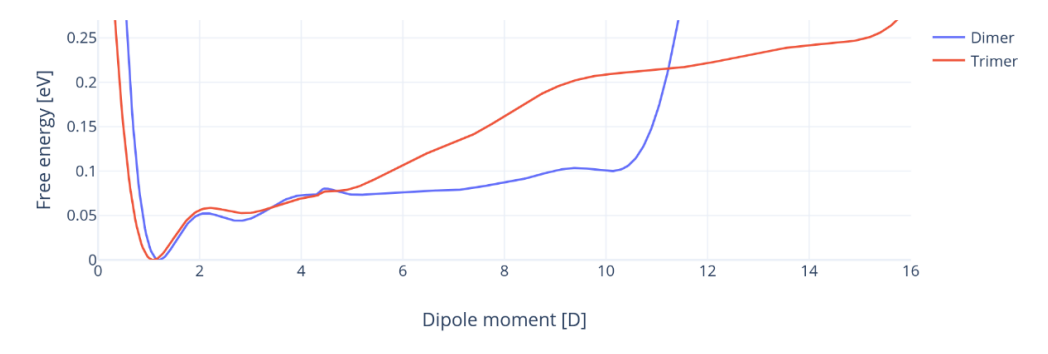


Figure S2. PMF for DMSO dimer and trimer complexes for the dipole moment coordinate at 100K.

# IV. Transition between two dimers at a distance and D5

Nudged elastic band (NEB) optimization<sup>S9</sup> was performed to find energy barriers between two DMSO molecules a distance apart (13.5 Å; in the minimal geometry at that separation the two DMSO molecules have aligned dipoles) and complex D5. Fig. S3 shows that the connection is barrierless.

The simulations were carried out in the TeraChem code S10,S11 using the B3LYP(D2)/aug-cc-pVDZ method with 14 molecular images between the two structures. The images were generated by constrained minimization.

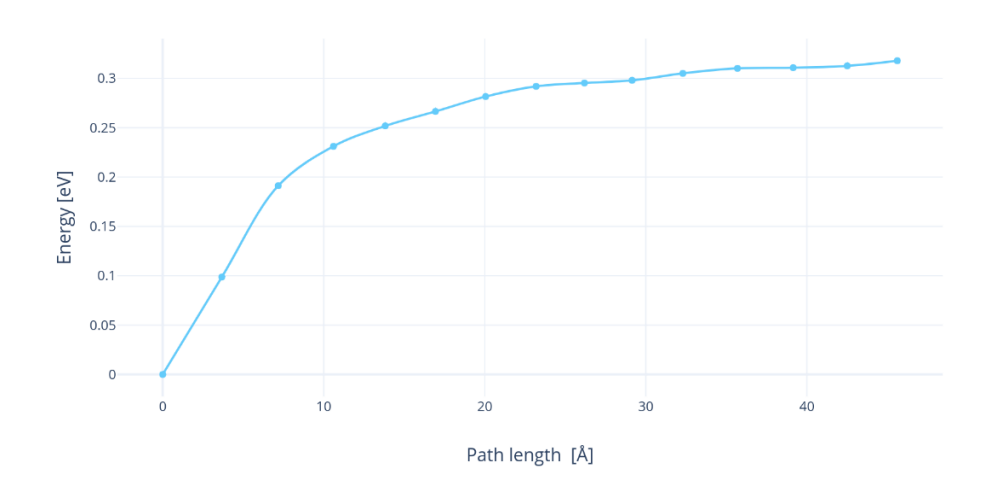


Figure S3. NEB calculations connecting the long-distance configuration to the D5 minimum.

# V. Transition between the D5 and D1 minima

We also performed NEB calculation connecting the D5 minimum with the global D1 minimum. The final energy curve is shown in Fig. S4.

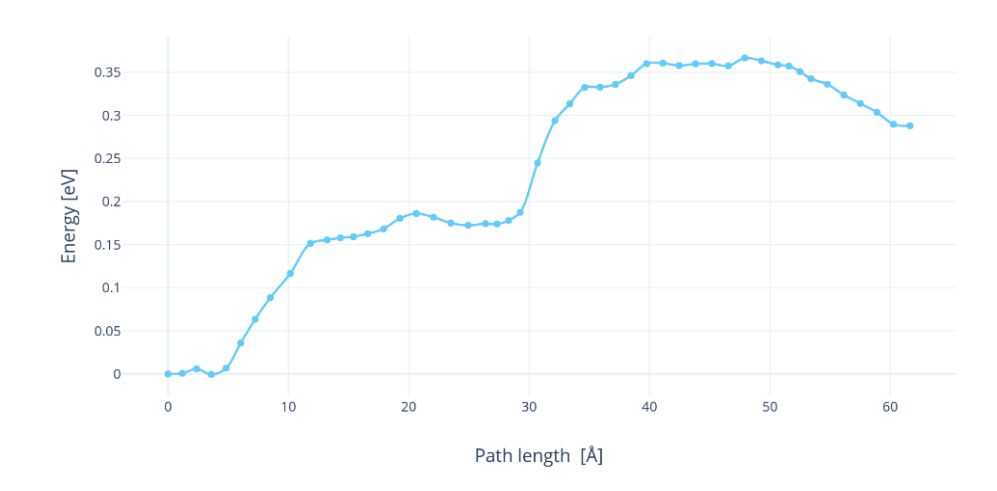


Figure S4. NEB calculations connecting the minima D1 and D5.

### VI. Two dimensional free energy surface

Additional insight into the topology of the multidimensional PES of DMSO aggregates can be brought about via modeling of free energy surfaces (FES). We evaluated the FES (i.e., the two dimensional version of the PMF in Fig. S2) as a function of two coordinates: the aggregate dipole moment and the interatomic S-S distance, see Figs. S5-S8. The graphs were once again generated using the metadynamics method and the temperature of 100 K to avoid convergence issues. It is clear that at large intermolecular distance the system prefers the high-dipole configuration, as mentioned above. At close distances one observes a number of minima separated by barriers.

The 2D metadynamics parameters were as follows. As before, for the dimer the simulation length was 100 ps, leap-frog stochastic integrator was utilized, the temperature was set to 100 K with thermostat constant  $\tau$ =1.0 ps. The first collective variable, CV1, was defined as the S-S interatomic distance between the DMSO monomers. An additional Gaussian potential was added at every 1000 steps. The Gaussian height was 0.015 kJ/mol and the CV1 Gaussian width was 0.1 nm. The second collective variable was the dipole moment with the same deposition parameters as CV1 and Gaussian width of 1.2 D. Upper energetic walls for CV1 were applied at 2 nm in order to keep the molecule in the area of interest.

For the trimer the simulation length was increased tenfold to 1000 ps, with the other parameters fixed. CV1 was redefined as the sum of S-S interatomic distances due to the presence of the third DMSO molecule, the other variables remained the same. The upper energetic walls for CV1 were shifted to 6.0 nm.

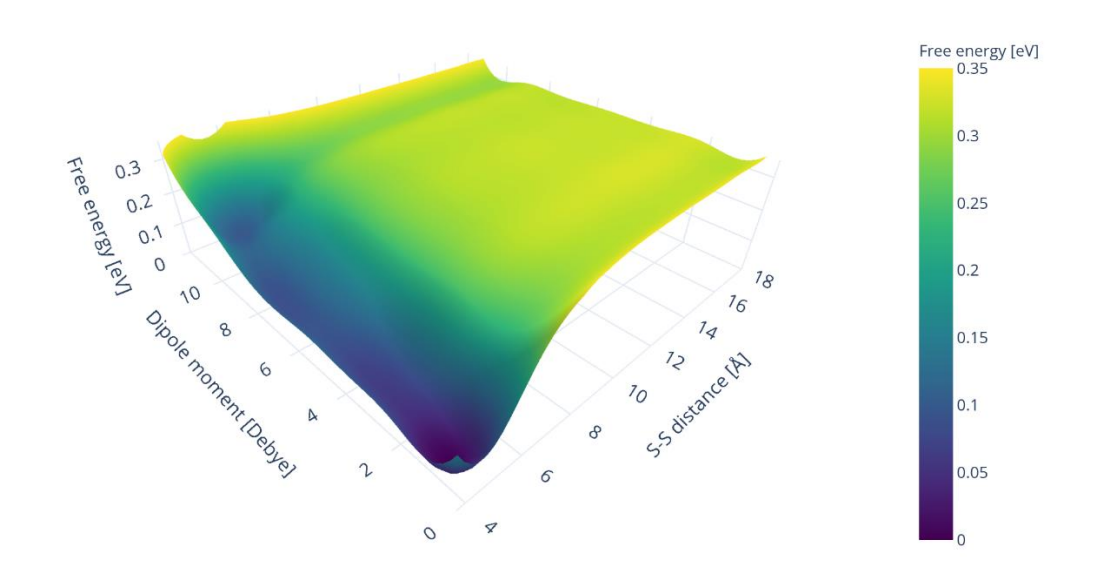


Figure S5. FES for the DMSO dimer at 100 K.

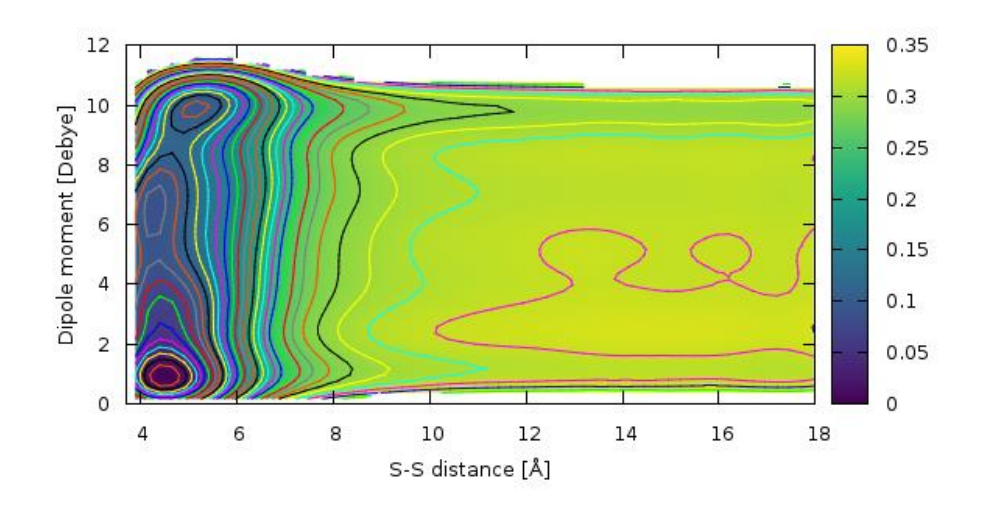


Figure S6. FES heatmap for the DMSO dimer at 100 K. Contour spacing 0.01 eV.

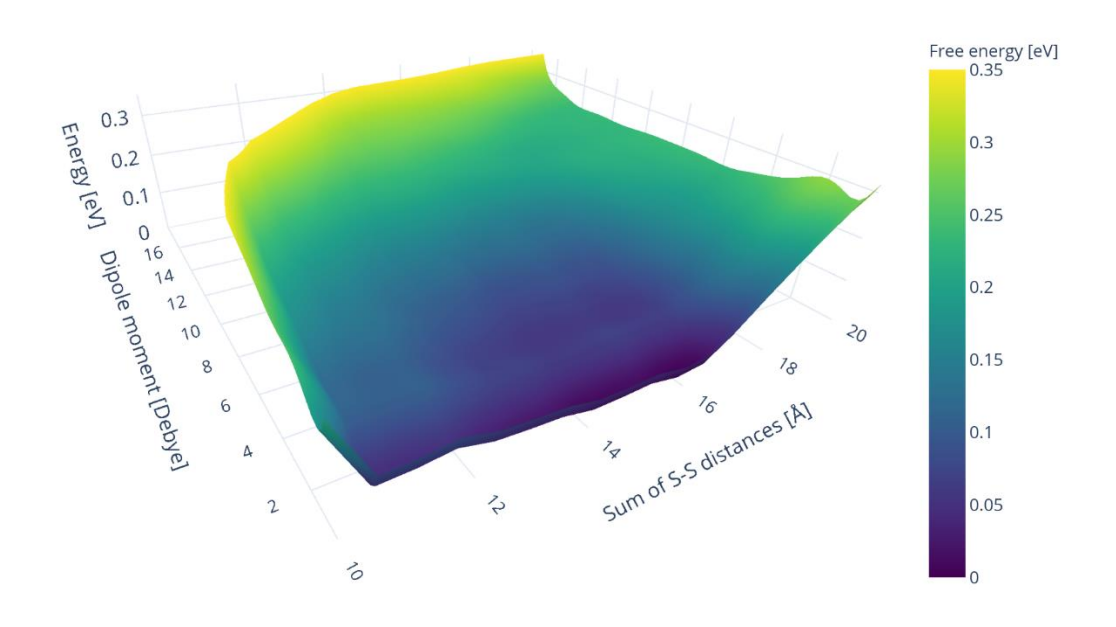


Figure S7. FES for the DMSO trimer at 100 K.

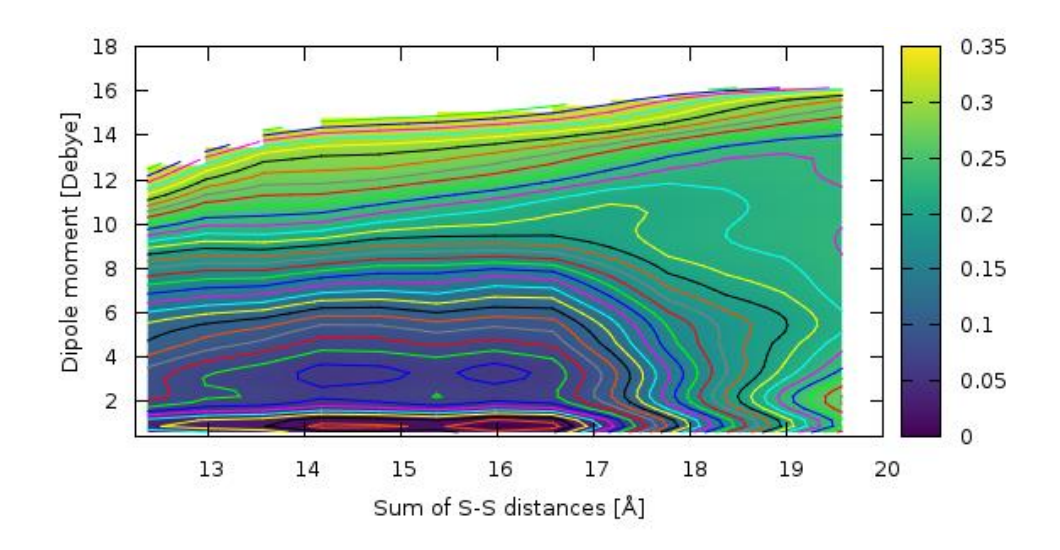


Figure S8. FES heatmap for the DMSO trimer at 100 K. Contour spacing 0.01 eV.

# VII. Force field parameters

The MM simulations were performed with parameters taken from ref S5. The parameters are summarized in Tables S2 and S3.

**Table S2.** Atomic type parameters for DMSO.

Atom	Charge	ε (kJ/mol)	σ (nm)
O	-0.556	0.50242	0.30291
S	0.312	1.46537	0.35636
C	-0.148	0.32657	0.36348
Н	0.090	0.10048	0.23876

**Table S3.** Intermolecular parameters for DMSO.

Bond	$b_0$ (nm)	$f_{\rm c}$ (kJ mol <sup>-1</sup> nm <sup>-2</sup> )
Н-С	0.111	134724.8
C-S	0.180	100416.0
S-O	0.153	225936.0

Angles	$\theta_0  (\mathrm{nm})$	$f_{\rm c}$ (kJ mol <sup>-1</sup> rad <sup>-2</sup> )
Н-С-Н	108.400	148.5320
H-C-S	111.300	192.8824
C-S-O	106.750	330.5360
C-S-C	95.000	142.2560

Dihedrals	$\varphi_0$ (deg)	f <sub>c</sub> (kJ mol <sup>-1</sup> )	X
H-C-S-O	0.0	0.8368	3
H-C-S-C	0.0	0.8368	3

### VIII. Cartesian coordinates of all structures

Geometries of the optimal structures presented in Figs. 2 and 4 of the main text are listed below, with all coordinates in Angstroms.

#### Monomer 10 C 1.390750 0.279323 -0.278296 S 0.072728 -0.679506 0.585004 C -1.342363 0.171624 -0.236526 O 0.075720 -0.189227 2.044957 H 1.346127 0.069130 -1.356470 H 1.227420 1.344812 -0.066434 H 2.347951 -0.053762 0.141464 H -1.314193 -0.035613 -1.315827 H -2.257159 -0.235280 0.211752 H -1.256995 1.246897 -0.028367 D1 20 С 1.391830 0.296071 -0.267191 S 0.073035 -0.689518 0.555023 C -1.343411 0.188626 -0.225497 O 0.078854 -0.256270 2.047129 H 1.379923 0.056354 -1.339642 H 1.179380 1.359143 -0.087564 H 2.341205 -0.018939 0.183566 H -1.345350 -0.050790 -1.298081 H -2.251051 -0.199163 0.253587 H -1.209576 1.265306 -0.051326 S -0.073081 3.587139 1.938615 O -0.078682 3.153903 0.446506 C -1.391839 2.601376 2.760682 C 1.343385 2.709142 2.719264 H -1.380080 2.841096 3.833135 H -2.341208 2.916257 2.309824 H -1.179218 1.538334 2.581077 1.345162 2.948483 3.791865 Η 1.209699 1.632459 2.545001 2.251033 3.097074 2.240313

8.826895 8.110270 10.400227 9.972464 S 7.608129 9.483674 11.539269 7.974326 10.379345 12.382316 7.730081 9.717863 11.525836 9.039717 Н 10.646509 Н 11.551024 7.328890 11.266521 C 10.186293 8.892506 8.183524 11.035534 8.602394 7.548535 9.256912 8.900193 7.600878 Н 9.852789 10.362717 8.687985 10.697510 11.161246 10.536141 S 9.253455 11.346438 11.076378 С 9.145789 10.330797 12.600760 8.213528 10.584098 13.124409 Н Н 9.133390 9.289859 12.256910 10.027135 10.559985 13.215271 Н C 9.274676 12.983721 11.916622 8.313117 13.137349 12.426572 Н Н 10.112562 12.992963 12.626663 Н 9.422581 13.740250 11.136213 D3 20 -6.599507 -9.935427 -8.808258 S -6.050826 -8.220930 -8.418528 -7.587463 -7.381111 -8.969174 -4.975044 -7.895873 -9.486073 -7.454125 -10.195223 -8.167596 -6.867985 -9.974321 -9.872589 -5.748550 -10.596439 -8.602335 -8.424339 -7.741197 -8.354184 H -7.407231 -6.311806 -8.806702 -7.734957 -7.620273 -10.031201 -4.736135 -4.653480 -8.965041 O -5.810347 -4.978975 -7.896071

C -4.188088 -2.938502 -8.576590

-2.678643

-2.277959

-2.898989

-5.133640

-5.251363

H -3.379470 -6.561814 -8.576431

-8.416137

-9.217880

-8.782326

-7.512438

-9.033730

-7.354870

-3.198394 -5.492320

-3.333958

-5.039455

-2.362832

-3.048402

H -3.918996

C

Н

Н

Н

2.491453

1.103863

1.450590

-0.098565

-4.765940

-4.786018

-2.071775

-2.774219

0.340792 -1.054444 -3.366810

-1.690035

-2.843846

-4.364292

-3.724319

O 10.770543 12.406453 7.172925 10.996603 12.217603 S 8.692035 11.452412 12.663048 8.865018 12.827871 11.198932 9.921240 12.692858 10.559951 Н 8.226519 13.389878 12.202747 8.531247 Н 10.042817 10.713973 C 9.163143 10.255542 10.475201 10.214216 8.982319 10.960304 9.031380 Н 10.346341 9.897937 8.494552 0 11.783311 8.009573 5.181466 S 11.481115 9.357691 5.867285 12.445813 10.642888 C 4.970928 12.145669 11.622494 Н 5.364081 Н 13.505277 10.435700 5.167309 12.228607 10.534564 Н 3.900118 C 9.828399 9.903572 5.270228 9.653478 Н 10.918986 5.647899 Н 9.840437 9.858877 4.173228 9.097072 Н 9.191144 5.672183 D5 20 0.832083 0.053205 0.687160 C S -0.018838 0.529481 -0.873482 S -2.573673 1.568387 -1.989863 С 0.721902 -2.067199 -3.541948 -1.624708 -0.272902 -0.470355 0 -0.252453 2.053432 -0.806970 0 0.449839 -2.770887 -0.938584 C 2.024752 -4.266109 -2.547539 Н 0.867295 -1.043176 0.726962 Н 1.838413 0.487869 0.644560 0.262499 0.486055 1.520395 Н Н -1.455444 -1.355871 -0.418903 -1.978107 0.143628 0.482340 Н Н -2.317341 -0.012725 -1.280529 2.733390 -4.189503 -3.384114 Н

```
18.325573 19.811653 21.617481
  19.721884
              20.312996
S
                         21.169378
   20.228323
              21.608815
                         22.376809
   21.215482
              21.985848
                         22.075579
   19.485068
              22.415686
                         22.369997
   20.289383
              21.113897
                         23.353709
   19.440363
              21.463757
                         19.758658
   20.418372
              21.838813
                         19.426676
  18.968548
              20.870817
                         18.965678
              22.289633
   18.799604
                         20.091628
   18.271096
              24.146530
                         21.392567
S
  17.718310
              25.601134
                         21.478337
   16.938575
              25.747636
C
                         23.136233
              26.754394
   16.505635
                         23.216988
   16.166283
              24.969074
                         23.217754
  17.742714
              25.618895
                         23.871189
Н
   16.151632
C
              25.602873
                         20.517245
   15.714781
              26.608754
                         20.587075
   16.422965
              25.376776
                         19.478677
  15.486136
              24.843390
                         20.952583
   14.642326
              23.527870
                         22.517495
  15.116812
              22.043647
                         22.457649
   16.675088
              21.971241
                         23.424806
   17.142014
              20.993610
                         23.248081
   17.321498
              22.778503
                         23.058847
   16.399735
              22.113636
                         24.476868
С
  15.887654
              21.824953
                         20.806281
   16.405169
              20.856910
                         20.796220
   15.074819
              21.866766
                         20.071118
   16.603161 22.645493
                         20.671394
```

T2 30

> C 19.978371 22.960022 19.710536 S 19.735892 23.242403 21.510328 C 20.388685 21.613064 22.058900 21.745112 0 18.198954 23.189838 15.358815 23.917374 20.096399 14.121084 23.111607 21.194225 C 15.047600 23.377434 22.762579 14.190395 21.590951 20.897064 0 17.054341 20.556144 20.208772 C 15.942352 19.217124 19.628149

O 18.501515 20.064915 19.893824 16.827935 20.251673 22.004302 21.059208 22.936455 19.512556 19.496985 22.004570 19.454354 19.514939 23.811524 Н 19.197357 21.467010 21.591478 21.848409 20.210845 21.552465 23.139753 19.850741 20.831749 21.503192 15.760191 20.345461 22.229074 17.216281 19.244890 22.206490 17.413863 21.021960 22.516917 14.919373 19.492859 19.911972 16.052332 19.168894 18.537795 16.267612 18.274891 20.088960 15.332881 24.997756 20.296283 Н 16.349231 23.496971 20.310933 Н 15.040118 23.707847 19.068112 15.045690 24.454363 22.980238 14.504377 22.828117 23.541197 Н 16.073387 23.010200 22.639216

T3 30

> C 19.318080 22.762136 22.418743 18.401131 21.379365 S 21.618767 18.852818 21.822207 19.888771 16.894078 21.701134 21.778298 0 19.025390 25.162225 20.116170 18.978878 26.478380 S 19.285963 С 18.218864 27.737277 20.375610 27.130948 20.695828 19.340978 16.290257 24.915699 22.126303 S 15.070039 25.136098 20.770491 15.850747 23.953991 19.603056 15.323351 26.555016 20.184537 22.293887 20.393691 22.575593 19.028486 23.706104 21.941314 22.740531 19.045684 23.480909 19.921248 21.605360 19.751253 Н 18.245550 21.181412 19.238001 18.646287 22.887366 19.725303 28.127033 20.713003 18.877545 Н 21.008893 27.173273 20.392785 21.324967 26.432136 18.776249 18.326517 28.718024 19.891996 17.157993 27.455148 20.467183

```
H 18.745592 27.706182 21.339379
  16.277900
             23.860237
                        22.428986
  17.274927
             25.192098
                        21.728825
Н
  15.980785
             25.581780
                        22.940796
   15.862931
             22.963479
Н
                        20.077728
  15.245255 23.967205
                        18.688986
  16.872837 24.307564 19.416185
```

T4 30

5.071517 -0.034670 -3.655985 S 4.287297 -0.194668 -1.997307 -1.075361 С 5.830416 -0.559251 3.893217 1.257561 -1.611793 0 S -0.020529 2.540318 0.295084 С 1.283159 3.066414 -0.885371 0 0.572434 2.732177 1.715202 C 3.644181 1.756288 1.598188 S 2.617946 0.269497 1.276626 C 1.964214 0.086045 2.982365 0 3.615924 -0.905124 1.078908 1.323627 0.953582 3.183548 1.388114 -0.847471 2.998202 Н 2.818493 0.022048 3.669544 2.968760 2.565559 1.900207 Н 1.495270 4.362207 2.386815 Н Н 4.148555 1.979398 0.651252 Н 0.822989 3.182558 -1.876460 4.020594 -0.522132 Н 1.688760 2.057413 2.289562 -0.920766 Н Н 5.497260 -1.005416 -3.946611 Н 4.282043 0.264332 -4.356496 0.740863 Н 5.846821 -3.594728 6.247662 -1.502562 -1.454190 Н 6.520679 0.279922 -1.237121 Н 5.523931 -0.655551 -0.027295 -1.126902 3.988674 0.041019 C -1.509237 3.972861 -0.989222 H -1.948976 3.889460 0.760368 -0.546405 4.899313 0.241051

16.634857 24.592189 18.933949 17.819686 24.188608 S 19.842340 18.546611 25.748060 20.487096 19.438384 25.480875 21.069767 18.776646 26.394312 19.630220 Н 17.780785 26.213377 21.119207 19.237765 23.746631 18.763679 20.096423 23.565749 19.425082 18.955755 22.836787 18.219781 24.574596 19.417204 18.065138 20.209226 23.485765 22.163446 S 18.877554 23.104769 22.864853 19.254372 22.812446 24.636229 C 18.324234 22.468296 25.107880 20.058270 22.067975 24.708308 19.577739 23.772502 25.056335 Н 18.574534 21.347602 C 22.430705 17.751416 20.981712 23.056223 18.299881 21.331231 21.369829 Н 19.512448 20.803987 22.601658 15.856035 22.403783 0 23.805490 15.408064 22.687282 22.347855 15.384240 24.514743 22.152187 15.163099 24.748814 21.101020 Н 14.647435 24.936357 22.847504 16.395863 24.844707 22.412702 С 13.585634 22.453003 22.322482 13.200021 22.813677 21.358789 13.395364 21.379488 22.440968 13.163459 23.017678 23.164279

T6 30

> O 18.248791 19.538962 25.445555 18.177691 19.442715 26.988687 18.433034 21.156221 27.613792 28.710183 18.496857 21.127477 19.356533 21.546423 27.166533 17.561677 21.740741 27.294830 C 19.813685 18.792657 27.529990 19.853766 18.804080 28.627823 Н 19.884199 17.765020 27.153619 20.593531 19.428978 27.091708

O 22.122928 22.013981 19.259183 S 22.029013 21.907157 20.795300 22.263129 23.603652 21.467768 H 22.337954 23.520943 22.560161 23.173825 24.017982 21.015392 Н 21.385740 24.187672 21.162752 C 23.639059 21.242274 21.387621 23.636418 21.292751 22.484521 23.704654 20.207811 21.027740 24.435317 21.852934 Н 20.941810 0 22.288179 21.938705 24.307074 S 21.002813 21.173364 24.716842 20.992990 19.611911 23.748124 20.049272 19.097423 23.964572 H 21.091252 19.874277 22.687275 21.857084 19.027672 24.087681 Н 19.609864 21.978664 23.829299 18.704772 21.397957 24.043202 H 19.535878 22.999435 24.224070 19.855097 21.990158 22.759892

T7 30

> C 0.472180 -0.265895 0.733682 S -0.136458 0.321670 -0.898489 O -0.384447 1.846400 -0.754727 C -1.785515 -0.482541 -0.798695 0 0.359320 -2.893610 -1.176365 S 1.641205 -2.693731 -2.021010 С 2.115524 -4.372107 -2.603230 C 1.077057 -2.055772 -3.650613 Н 0.551026 -1.358283 0.675742 Н 1.451728 0.200982 0.892637 -0.247228 0.058360 1.495983 Н -1.625451 -1.566818 -0.828784 Н -2.261186 -0.155086 0.134675 -2.355211 -0.137931 -1.670337 Н Н 2.951015 -4.283369 -3.311612 Н 2.420451 -4.939134 -1.715311 Н 1.234961 -4.831777 -3.071533 1.927235 -2.048859 -4.346467 Н Н 0.268384 -2.708093 -4.006330 Η 0.713231 -1.036965 -3.472756 S -2.320128 1.993864 2.169713 0 -3.154515 2.294445 3.432453 C -3.077491 2.942538 0.787412

```
C -0.788980
              3.007148
                         2.285051
H -2.419933
              2.841894
                        -0.086210
  -4.064898
              2.499581
                         0.606587
H -3.180753
              3.985061
                         1.116591
  -0.254575
Н
              2.912504
                         1.330540
  -1.090007
              4.041603
                         2.496975
H -0.204794
              2.601451
                         3.120616
```

T8 30

O 22.134918 25.903523 23.940447 S 23.041269 24.808338 24.561304 C 22.070844 24.071469 25.935851 22.726180 23.402398 26.509576 H 21.686789 24.890733 26.558087 21.251172 23.507444 25.474200 C 24.246540 25.712157 25.614598 24.984221 26.187314 24.837479 24.891884 26.286350 24.938904 23.682050 26.382530 26.276309 0 18.026224 22.657810 23.136880 19.327282 23.413547 23.474273 18.847931 25.002640 24.270183 19.769957 25.568621 24.458552 Н 18.190563 25.554032 23.588146 18.338681 24.736761 25.204821 C 19.960394 24.149959 21.912549 Н 20.865655 24.718669 22.164650 23.308764 21.246021 20.186067 19.190316 24.810736 21.496604 0 18.606089 27.152941 21.810753 S 19.594310 28.340832 21.800217 21.206535 27.678398 21.199666 21.938315 28.498325 21.206754 Н 21.524346 26.861633 21.859709 Н 21.033168 27.327994 20.175000 20.127602 28.590982 23.547016 20.862715 29.407639 23.569519 Н 19.226795 28.869318 24.107320 H 20.565929 27.657234 23.920780

### References

- S1 *CRC Handbook of Chemistry and Physics*, 99<sup>th</sup> edition, ed. J. R. Rumble, CRC Press, Boca Raton, 2018
- S2 D. Hait, M. Head-Gordon, J. Chem. Theory Comput. 2018, 14, 1969.
- M. J. Frisch, G. W. Trucks, H. B. Schlegel, G. E.Scuseria, M. A. Robb, J. R. Cheeseman, G. Scalmani, V. Barone, B. Mennucci, G. A. Petersson, H. Nakatsuji, M. Caricato, X. Li, H. P. Hratchian, A. F. Izmaylov, J. Bloino, G. Zheng, J. L. Sonnenberg, M. Hada, M. Ehara, K. Toyota, R. Fukuda, J. Hasegawa, M. Ishida, T. Nakajima, Y. Honda, O. Kitao, H. Nakai, T. Vreven, J. A. Montgomery, Jr., J. E. Peralta, F. Ogliaro, M. Bearpark, J. J. Heyd, E. Brothers, K. N. Kudin, V. N. Staroverov, R. Kobayashi, J. Normand, K. Raghavachari, A. Rendell, J. C. Burant, S. S. Iyengar, J. Tomasi, M. Cossi, N. Rega, J. M. Millam, M. Klene, J. E. Knox, J. B. Cross, V. Bakken, C. Adamo, J. Jaramillo, R. Gomperts, R. E. Stratmann, O. Yazyev, A. J. Austin, R. Cammi, C. Pomelli, J. W. Ochterski, R. L. Martin, K. Morokuma, V. G. Zakrzewski, G. A. Voth, P. Salvador, J. J. Dannenberg, S. Dapprich, A. D. Daniels, Ö. Farkas, J. B. Foresman, J. V. Ortiz, J. Cioslowski and D. J. Fox, Gaussian 09 (Rev. D.01), Gaussian, Inc., Wallingford, CT, 2009.
- S4 B. Aradi, B. Hourahine and Th. Frauenheim, J. Phys. Chem. A. 2007, 111, 5678.
- S5 M. L.Strader and S. E. Feller, *J. Phys. Chem. A.* 2002, **106**, 1074.
- S6 A. Barducci, M. Bonomi and M. Parrinello, WIREs Comput. Mol. Sci. 2011, 1, 826.
- S7 M. J. Abraham, T. Murtola, R. Schulz, S. Páll, J. C. Smith, B. Hess and E. Lindahl, *SoftwareX* 2015, **1-2**, 19.
- S8 G. A. Tribello, M. Bonomi, D. Branduardi, C. Camilloni and G. Bussi, *Comput. Phys. Commun.* 2014, **185**, 604.
- S9 H. Jonson, G. Mills and K. W. Jacobsen, in *Classical and Quantum Dynamics in Condensed Phase Simulations*, ed. B. J. Berne, G. Ciccotti and D. F. Coker, World Scientific, Singapore, 1998, pp. 385-404.
- S10 TeraChem v 1.9. http://www.petachem.com.
- S11 I. S. Ufimtsev and T. J. Martinez, J. Chem. Theory Comput. 2009, 5, 2619.